Nonlinear Dyn (2012) 69:1063–1079
DOI 10.1007/s11071-012-0327-0

ORIGINAL PAPER

On intentional introduction of stiffness nonlinearities for energy harvesting under white Gaussian excitations

Mohammed F. Daqaq

Received: 8 July 2011 / Accepted: 10 December 2011 / Published online: 20 January 2012

Abstract A significant body of the open literature on vibratory energy harvesting is currently focused on the concept of purposeful inclusion of stiffness nonlinearities for broadband transduction. When compared to their linear resonant counterparts, nonlinear energy harvesters have a wider steady-state frequency bandwidth, leading to the idea that they can be utilized to improve performance especially in random and non-stationary vibratory environments. To further investigate this common belief, this paper studies the response of vibratory energy harvesters to white Gaussian excitations. Both mono- and bi-stable piezoelectric Duffing-type harvesters are considered. The Fokker–Plank–Kolmogorov equation governing the evolution of the system's transition probability density function is formulated and used to generate the moment differential equations governing the response statistics. The moment equations are then closed using a fourth-order cumulant-neglect closure scheme and the relevant steady-state response statistics are obtained. It is demonstrated that the energy harvester's time constant ratio, i.e., the ratio between the nominal period of the mechanical subsystem and the time constant of the harvesting circuit, plays a critical role in characterizing the performance of nonlinear harvesters in a random environment. When the time constant ratio is large, stiffness-type nonlinearities have very little influence on the voltage response. In such a case, no matter how the potential function of the harvester is altered, it does not affect the average output power of the device. When the time constant ratio is small, the influence of the nonlinearity on the voltage output becomes more prevalent. In this case, a Duffing-type mono-stable harvester can never outperform its linear counterpart. A bi-stable harvester, on the other hand, can outperform a linear harvester only when it is designed with the proper potential energy function based on the known noise intensity of the excitation. Such conclusions hold for harvesters with nonlinearities appearing in the restoring force.

Keywords Energy harvesting · Random · Nonlinear · White

M.F. Daqaq (✉)
Nonlinear Vibrations and Energy Harvesting Lab. (NOVEHL), Department of Mechanical Engineering, Clemson University, Clemson, SC 29634, USA
e-mail: mdaqaq@clemson.edu

1 Introduction

With the increased interest in vibratory energy harvesting, especially for powering remote sensors and other inaccessible low-power consumption electronics; many research studies are currently focused on developing technologies to enhance their efficacy. Of a special importance is the development of harvesters that can scavenge energy efficiently from non-stationary and random excitation sources. This has recently become a more pressing issue, especially, with

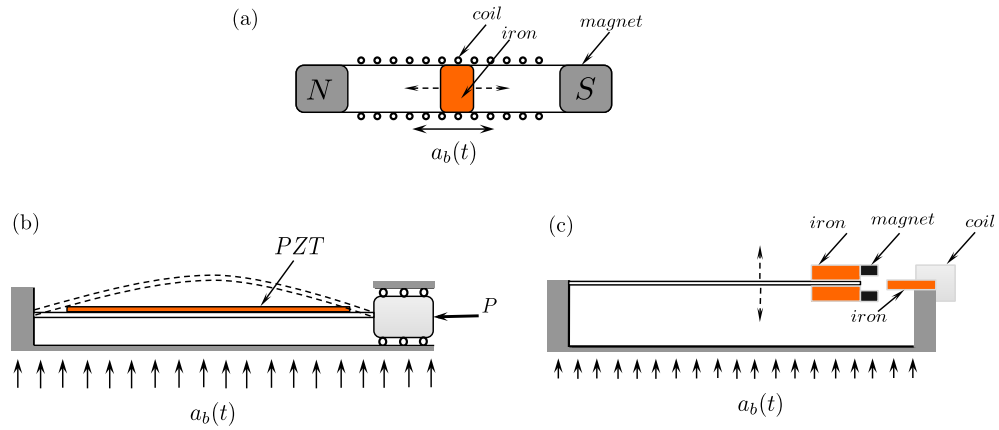

Fig. 1 Schematics of different nonlinear tunable energy harvesters. (**a**), (**c**) Inductive VEHs proposed in [11, 21] and [10], respectively; the linear stiffness and nonlinearity can be tuned by varying the distance between the magnets. (**b**) Piezoelectric VEH proposed in [12]; linear stiffness and nonlinearity can be tuned by varying an axial load, P. All devices can operate in the mono- and bi-stable configurations and $a_b(t)$ refers to the environmental base excitation

the knowledge that such excitations represent a large segment of the available environmental vibratory energy sources.

Almost a decade ago when vibratory energy harvesting started to shape and evolve [1], energy harvesters were generally linear with a fixed frequency. Such designs have a narrow frequency bandwidth, and, hence, operate efficiently only when the excitation source has a fixed frequency that is close to the fundamental frequency of the harvester (resonance condition). Small variations in the excitation frequency around the harvester's fundamental frequency cause the already small energy output of the harvester to drop even further, thereby making the energy harvesting process inefficient. As a result, it was soon realized that such devices cannot be used to harvest energy from excitations that have time-dependent or broadband characteristics in which the energy is distributed over a wide spectrum of frequencies or the dominant frequencies vary with time.

To remedy this problem, some initial solutions called for the design of vibratory energy harvesters (VEHs) with tunable characteristics. Tunability mechanisms use passive/active design means to alter the fundamental frequency of the harvester to match the dominant frequency of the excitation [2–8]. Following a number of research investigations, it became evident that tunable VEHs can only be utilized to account for slow drifts in the excitation's frequency and are not efficient under random or fast-varying frequency inputs [2]. In addition, tuning mechanisms usually require external power or complex design means which reduces the power density and adversely influences the scalability of the harvester.

During the last couple of years, many researchers have also exploited purposefully introducing stiffness-type nonlinearities into the harvester's design. This has the influence of extending the coupling between the environmental excitation and the harvester to a wider range of frequencies [9–20]. There are two different classes of these harvesters. The first is designed to exhibit a nonlinear resonant behavior similar to that of a *mono-stable Duffing oscillator* with a hardening/softening nonlinearity [10–12]. Examples of such VEHs include, but are not limited to, the magnetically-levitated inductive harvester proposed by Mann and Sims [11] and shown in Fig. 1(a). This harvester comprises two outer magnets to levitate a fluctuating central magnet. The nonlinearity is introduced in the form of the magnetic restoring force, which also enables the system to be tuned to a specific resonant frequency. Per Faraday's law, energy is generated as a result of the relative motion between the coil and the center magnet. Barton et al. [10] also proposed a mono-stable inductive VEH but in the form of a tip magnet attached to a cantilever beam, Fig. 1(c). When the beam oscillates, the magnet moves relative to a coil wound around an iron core generating a current in the coil.

Masana and Daqaq [12] also proposed a mono-stable axially-loaded piezoelectric clamped–clamped

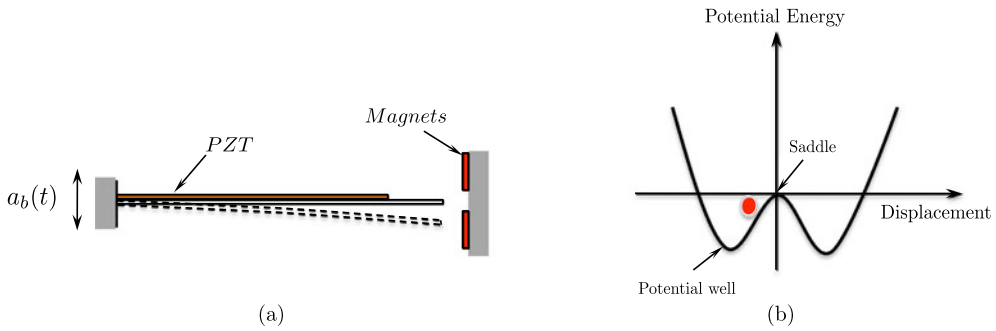

Fig. 2 (**a**) Schematic of a bi-stable piezoelectric harvester. (**b**) Associated potential energy function

beam harvester as shown in Fig. 1(b). The axial preload, which is kept below the critical buckling load, serves to tune the natural frequency of the beam and to introduce a cubic nonlinearity which depends on the magnitude of the axial load. The device harvests energy as a result of the excitation-induced deformation of a piezoelectric patch attached to the surface of the beam.

The second class of nonlinear harvesters is designed to have a double-well potential energy function exhibiting the response of a *bi-stable Duffing oscillator* as shown in Fig. 2(b). The operation concept of this class, which has been initially proposed by Cottone et al. [15] and later studied by several researchers [9, 10, 12, 14, 17], is based on the widely-celebrated bi-stable magneto-elastic structure of Moon and Holmes [22]. While several variances of the device were proposed, the main concept of operation is very similar. As shown in Fig. 2(a), the device consists of a piezoelectric beam (harvester) with a ferroelectric tip oscillating between two magnets. For a certain separation range between those magnets, the system becomes bi-stable having a *double-well* potential energy function with two stable equilibria and one unstable saddle. It has been shown that, under some conditions in which the inter-well dynamics of these VEH is activated, such devices can yield a broadband output power under steady-state fixed-frequency harmonic excitations [14, 17].

Masana and Daqaq [23] also investigated the response of a bi-stable VEH based on the axially-loaded clamped–clamped piezoelectric beam design. In this case, however, the axial load is increased beyond the critical buckling load to create the bi-stable potential. They compared the response of the bi-stable configuration to the mono-stable one under harmonic fixed-frequency excitations illustrating that the bi-stable harvester can *only* outperform the mono-stable design for some shapes of the potential energy function and for large base excitation levels. They also studied the response of the bi-stable harvester in the vicinity of the super-harmonic resonance of order two demonstrating that it can offer unique capabilities to harvest energy under low-frequency excitations [24].

While the purposeful introduction of nonlinearities has been aimed to resolve the issue of excitations' non-stationarities and randomness, the associated analyses and predicted power enhancements were, for the most part based, on the steady-state response which assumes a harmonic fixed-frequency excitation. As of today, we still do not have a clear understanding of how the nature of excitation influences the output power, or what role stiffness nonlinearities play in the transduction of energy harvesters under random excitations. Still, it is not even well-understood whether the steady-state fixed-frequency analysis currently adopted in the literature is a valid performance indicator.

A few recent papers have tried to address some of these unanswered questions by providing a clearer picture of how randomness and non-stationarities in the excitation influence the average power of VEHs. In one demonstration, Adhikari et al. [25] studied the response of linear piezoelectric VEHs to white Gaussian excitations. Using an analytical approach, Osorio and Daqaq [26] analyzed the response of linear piezoelectric VEHs to sinusoidally-varying frequency excitations. Barton et al. [27] investigated experimentally the response of a mono-stable inductive VEH to random band-limited excitations showing that the nonlinearity does not improve the output power. Daqaq [28] used an analytical approach based on the Van Kampen ex-

pansion to demonstrate that, under white Gaussian excitations, an inductive Duffing-type mono-stable harvester produces the same amount of power as its linear counterpart. He also showed that the nonlinearity can only reduce the average power under band-limited random Gaussian noise.

The response of a nonlinear piezoelectric VEHs to white Gaussian excitations was also numerically and experimentally investigated by Gammaitoni et al. [29]. Additionally, Daqaq [30] used an approximate analytical solution of the Fokker–Plank–Kolmogorov (FPK) equation to analyze the response of a bi-stable inductive VEH to white and exponentially-correlated Gaussian noise. In his previous studies [28, 30], the author assumed that the inductance of the harvesting circuit can be neglected which allowed for reducing the system into a single second-order oscillator with an effective damping term. This lead to the conclusion that the nonlinearity has no influence on the output voltage under white Gaussian excitations.

In this paper, more light is shed onto the influence of nonlinearities on piezoelectric energy harvesting under white Gaussian excitations where the effective capacitance of the piezoelectric element cannot be neglected, and, hence, the system cannot be reduced into a single second-order oscillator with an effective damping term as in [28, 30]. With that, the paper focuses on the relative performance of nonlinear energy harvesters when compared to their linear counterparts and identifies the design conditions and noise intensities under which a nonlinear harvester can actually outperform a linear one. Section 2 presents a generic lumped-parameter model which can capture the qualitative behavior of piezoelectric energy harvesters. Section 3 formulates the problem in the Itô stochastic sense and presents the FPK equation governing the evolution of the transition probability density function (PDF). Section 4 solves the FPK equation analytically for a linear VEH and obtains analytical expressions for the relevant response statistics. Section 5 uses a non-Gaussian fourth-order cumulant neglect closure scheme to approximately solve the FPK equation in the case of the mono- and bi-stable harvesters, respectively. Resulting solutions are then utilized to study variations of the mean square voltage and average power with different system and excitation parameters including the nonlinearity, the time constant ratio, and the excitation's level. Results are also compared against those obtained in the linear scenario and discussions are presented to delineate the relative performance and the influence of the nonlinearity on the average power. Section 6 presents an analytical treatment for the special case of a large time constant ratio. Finally, Section 7 presents the important conclusions.

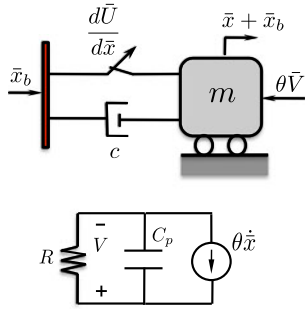

Fig. 3 A simplified representation of a piezoelectric energy harvester

2 Basic model

The mathematical model adopted in this study represents the dynamics of a generic capacitive (piezoelectric) vibratory energy harvester, which, as shown in Fig. 3, can be reduced to a base-excited spring–mass–damper system coupled to a capacitive energy harvesting circuit [31]. The equations governing the motion can be expressed as

$$\begin{aligned} m\ddot{\bar{x}} + c\dot{\bar{x}} + \frac{\mathrm{d}\bar{U}(\bar{x})}{\mathrm{d}\bar{x}} + \theta\bar{V} &= -m\ddot{x}_b, \\ C_p\dot{\bar{V}} + \frac{\bar{V}}{R} &= \theta\dot{\bar{x}}, \end{aligned} \tag{1}$$

where the dot represents a derivative with respect to time, τ. The variable $\bar{x}$ represents the displacement of the mass m; c is a linear viscous damping coefficient; θ is a linear electromechanical coupling coefficient; $\bar{V}$ is the voltage measured across an equivalent resistive load, R; $\ddot{x}_b$ is the base acceleration, and C_p is the piezoelectric capacitance. The function $\bar{U}(\bar{x})$ represents the potential energy of the mechanical subsystem and is given in the following general form:

$$\bar{U}(\bar{x}) = \frac{1}{2}k_1(1-r)\bar{x}^2 + \frac{1}{4}k_2\bar{x}^4, \tag{2}$$

where k_1 and k_2 are, respectively, a linear and nonlinear stiffness coefficients, and r is introduced to permit tuning of the linear stiffness around its nominal

value using external design means such as the axial load in the axially-loaded VEH proposed by Masana and Daqaq [12], Fig. 1(b), or the magnetic field as in the magnetically-tuned VEHs proposed in [11, 21, 27], Fig. 1(a), (c). Introduction of this constant is essential to reflect the fact that, for physical VEHs, the nonlinear coefficient cannot be easily changed without altering the linear stiffness due to physical and design constraints.

The equations of motion can be further non-dimensionalized by introducing the following transformations:

$$x = \frac{\bar{x}}{l_c}, \qquad t = \tau\omega_n, \qquad V = \frac{C_p}{\theta l_c}\bar{V}, \tag{3}$$

where l_c is a length scale chosen here to be the ratio between the area of the equivalent piezoelectric capacitor and the distance between its parallel plates, and $\omega_n = \sqrt{k_1/m}$ is the short-circuit natural frequency of the harvester. With these transformations, the non-dimensional equations of motion can be expressed as

$$\begin{aligned} &\ddot{x} + 2\zeta\dot{x} + \frac{\mathrm{d}U}{\mathrm{d}x} + \kappa^2 V = -\ddot{x}_b, \\ &\dot{V} + \alpha V = \dot{x}, \end{aligned} \tag{4}$$

where

$$\frac{\mathrm{d}U}{\mathrm{d}x} = (1-r)x + \delta x^3, \tag{5}$$

and

$$\begin{aligned} &\zeta = \frac{c}{2\sqrt{k_1 m}}, \qquad \kappa^2 = \frac{\theta^2}{k_1 C_p}, \\ &\alpha = \frac{1}{RC_p\omega_n}, \qquad \delta = \frac{k_2 l_c^2}{k_1}. \end{aligned} \tag{6}$$

Here ζ is the mechanical damping ratio, κ is a linear dimensionless electromechanical coupling coefficient, α is the ratio between the mechanical and electrical time constants of the harvester. The mechanical time constant being the reciprocal of the harvester's nominal frequency, ω_n; and the electrical time constant being that associated with the RC circuit of the harvester. Finally, δ is the coefficient of cubic nonlinearity. With these definitions, energy harvesters can now be classified into three major categories based on the shape of their potential energy function, Fig. 4. The harvester is considered to be linear mono-stable when $\delta = 0$ and $r < 1$, nonlinear mono-stable when $\delta > 0$ and $r \leq 1$, and nonlinear bi-stable when $\delta > 0$ and $r > 1$.

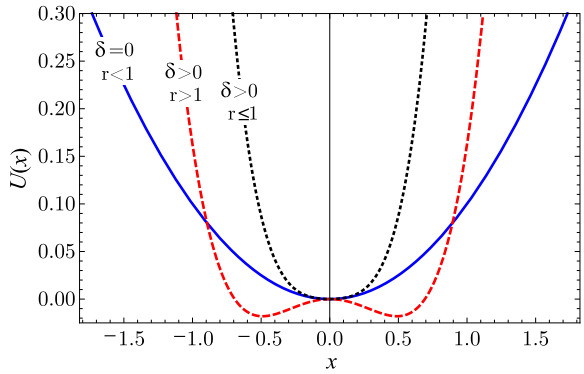

Fig. 4 Energy potentials associated with different types of energy harvesters

3 Fokker–Plank–Kolmogorov equation

Throughout this study, the environmental base excitation, $\ddot{x}_b$, is assumed to be a physical Gaussian process with a very small correlation time which approaches zero. In such a case, $\ddot{x}_b$ can be approximated by a Gaussian white noise process such that

$$\langle \ddot{x}_b(t) \rangle = 0, \quad \langle \ddot{x}_b(t)\ddot{x}_b(s) \rangle = \sigma^2 \hat{\delta}(s-t), \tag{7}$$

where $\langle\cdot\rangle$ denotes the expected value, σ^2 is the variance of the process, and $\hat{\delta}$ is the Dirac-delta function. To generate the response statistics associated with the stochastic dynamics of (4), we further express it in the Itô stochastic form as [32, 33]

$$\mathrm{d}\mathbf{x}(t) = \mathbf{f}(\mathbf{x}, t)\,\mathrm{d}t + \mathbf{G}(\mathbf{x}, t)\,\mathrm{d}\mathbf{B}, \tag{8}$$

where $\mathbf{x} = (x_1, x_2, x_3)^T \equiv (x, \dot{x}, V)^T$, B is a Brownian motion process such that $\ddot{x}_b(t) = \mathrm{d}\mathbf{B}/\mathrm{d}t$ and

$$\begin{aligned} \mathbf{f}(\mathbf{x}, t) &= \begin{Bmatrix} x_2 \\ -2\zeta x_2 - \frac{\mathrm{d}U}{\mathrm{d}x_1} - \kappa^2 x_3 \\ -\alpha x_3 - x_2 \end{Bmatrix}, \\ \mathbf{G}(\mathbf{x}, t) &= \begin{Bmatrix} 0 \\ -1 \\ 0 \end{Bmatrix}. \end{aligned} \tag{9}$$

The solution of (8) is determined by the evolution of the transition PDF, $P(\mathbf{x}, t)$, which, in turn, is governed

by the following FPK equation:

$$\frac{\partial P(\mathbf{x},t)}{\partial t} = -\sum_{i=1}^{3}\frac{\partial}{\partial x_i}\big[P(\mathbf{x},t)\mathbf{f}_i(\mathbf{x},t)\big] + \frac{1}{2}\sum_{i=1}^{3}\sum_{j=1}^{3}\frac{\partial^2}{\partial x_i x_j}\big[P(\mathbf{x},t)(\mathbf{Q}\mathbf{G}\mathbf{G}^T)_{ij}\big],$$
$$P(\infty,t) = P(-\infty,t) = 0, \tag{10}$$

where

$$\mathbf{Q} = \begin{bmatrix} 0 & 0 & 0 \\ 0 & \sigma^2 & 0 \\ 0 & 0 & 0 \end{bmatrix}.$$

With the knowledge of $\mathbf{f}(\mathbf{x},t)$ and $\mathbf{G}(\mathbf{x},t)$, the FPK equation reduces to

$$\frac{\partial P(\mathbf{x},t)}{\partial t} = -x_2\frac{\partial P(\mathbf{x},t)}{\partial x_1} + 2\zeta\frac{\partial (x_2 P(\mathbf{x},t))}{\partial x_2} + \left(\frac{\mathrm{d}U}{\mathrm{d}x_1} + \kappa^2 x_3\right)\frac{\partial P(\mathbf{x},t)}{\partial x_2} + \alpha\frac{\partial (x_3 P(\mathbf{x},t))}{\partial x_3} + x_2\frac{\partial P(\mathbf{x},t)}{\partial x_3} + \frac{\sigma^2}{2}\frac{\partial^2 P(\mathbf{x},t)}{\partial^2 x_2},$$
$$P(\infty,t) = P(-\infty,t) = 0. \tag{11}$$

Upon solving (11) for $P(\mathbf{x},t)$, the response statistics can then be obtained via

$$\left\langle \prod_{i=1}^{3} x_i^{k_i} \right\rangle = \int_{-\infty}^{\infty}\int_{-\infty}^{\infty}\int_{-\infty}^{\infty}\prod_{i=1}^{3} x_i^{k_i} P(\mathbf{x},t)\,\mathrm{d}x_1\,\mathrm{d}x_2\,\mathrm{d}x_3, \tag{12}$$

where $k_i = 0, 1, 2, \ldots$.

4 Energy harvesters with a linear restoring force

For the purpose of performance comparison, we start by investigating the response of the linear harvester ($\delta = 0$, $r < 1$). Since steady-state response statistics are of particular relevance for energy harvesting, we focus our attention on obtaining the stationary solutions of (11). In such a scenario, the transition probability function is time invariant, i.e., $\partial P(\mathbf{x},t)/\partial t = 0$ or $P(\mathbf{x},t) = P(\mathbf{x})$. Also, since for linear systems, the response to a Gaussian input is also Gaussian, it becomes possible to obtain an exact solution of (11) in the general Gaussian form

$$P(x_1,x_2,x_3) = A\exp\left(\sum_{i,j=1}^{3} a_{ij}x_i x_j\right), \tag{13}$$

where A is a constant obtained via the following normalization scheme:

$$\int_{-\infty}^{\infty}\int_{-\infty}^{\infty}\int_{-\infty}^{\infty} P(x_1,x_2,x_3)\,\mathrm{d}x_1\,\mathrm{d}x_2\,\mathrm{d}x_3 = 1, \tag{14}$$

and the a_{ij} are attained by substituting (13) into (11), then forcing the solvability conditions. This yields

$$a_{ij} = -\frac{1}{2}\frac{|D|_{ij}}{|D|}, \tag{15}$$

where

$$D = \frac{\sigma^2}{2\zeta(1-r+\alpha^2+2\alpha\zeta)+\kappa^2(\alpha+2\zeta)} \times \begin{bmatrix} \frac{1-r+\alpha^2+2\alpha\zeta}{1-r} & 0 & \frac{1}{2} \\ 0 & \frac{1-r+\alpha^2+2\alpha\zeta+\kappa^2}{2} & \frac{\alpha}{2} \\ \frac{1}{2} & \frac{\alpha}{2} & \frac{1}{2} \end{bmatrix}.$$

Here, $|D|$ and $|D|_{ij}$ represent, respectively, the determinant and co-factors of D.

With the knowledge of the exact stationary probability function, the required response moments can now be obtained using (12). Of special importance are the mean square values of the displacement, velocity, and voltage which can be expressed as

$$\langle x_1^2\rangle = \frac{\sigma^2}{1-r} \times \frac{1-r+\alpha^2+2\alpha\zeta}{2\zeta(1-r+\alpha^2+2\alpha\zeta)+\kappa^2(\alpha+2\zeta)}, \tag{16a}$$

$$\langle x_2^2\rangle = \frac{\sigma^2}{2} \times \frac{1-r+\alpha^2+2\alpha\zeta}{2\zeta(1-r+\alpha^2+2\alpha\zeta)+\kappa^2(\alpha+2\zeta)}, \tag{16b}$$

$$\langle x_3^2\rangle = \frac{\sigma^2}{2} \times \frac{1}{2\zeta(1-r+\alpha^2+2\alpha\zeta)+\kappa^2(\alpha+2\zeta)}. \tag{16c}$$

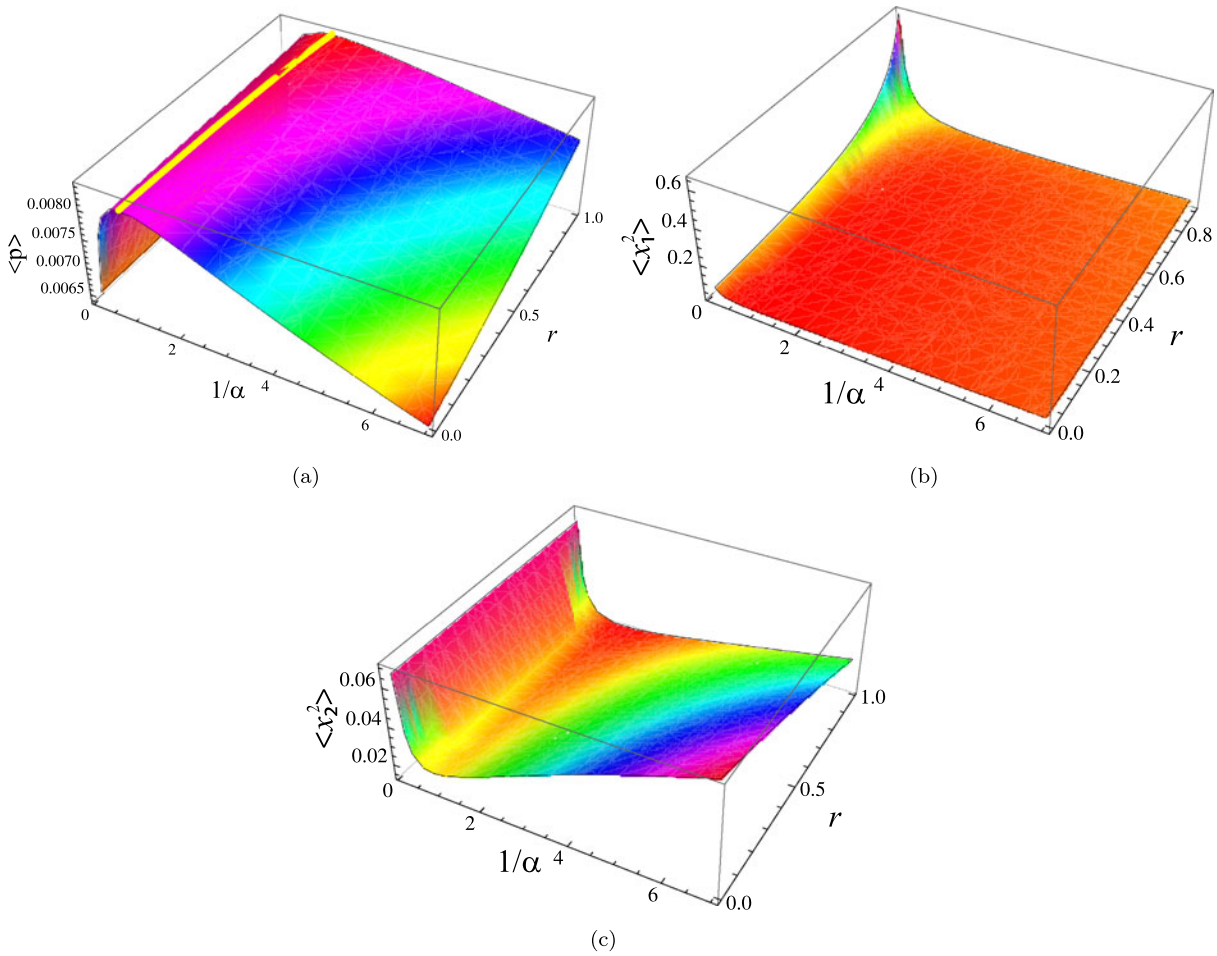

Fig. 5 Variation of the (**a**) power, (**b**) displacement, and (**c**) mean square values of the velocity with $1/\alpha$ and r for $\sigma = 0.1$, $\zeta = 0.01$, and $\kappa = 0.75$

Using (16c), a non-dimensional expression for the average power can now be expressed in the simple form

$$\langle \mathrm{p} \rangle = \frac{\langle \bar{\mathrm{p}} \rangle}{\mathrm{p}_o} = \alpha \langle x_3^2 \rangle, \tag{17}$$

where $\mathrm{p}_o = k_1 \omega_n \kappa^2 l_c^2$.

Using the resulting analytical expressions, (16a)–(17), we can now investigate the influence of the inverse time constant ratio (proportional to the load resistance) and the stiffness tuning constant, r, on the average power as well as the mean square values of the velocity and displacement. Figure 5(a) demonstrates that, similar to a deterministic excitation, the power increases initially as the load resistance is increased, exhibits a maximum at an optimal load resistance and drops again beyond the optimal value. The optimal time constant ratio, α_{opt}, can be obtained by finding the extremum of (17) with respect to α. This yields

$$\alpha_{\mathrm{opt}} = \sqrt{1 - r + \kappa^2}, \quad r \leq 1. \tag{18}$$

Since white noise has equal intensity in the spectral domain, the optimization results simplify significantly as compared to their deterministic harmonic counterparts. As evident in (18), the optimal time constant ratio is only dependent on r and κ and does not depend on the system mechanical damping ratio. Furthermore, under deterministic excitations, optimization results yield two optimal excitation frequencies known as the resonance and anti-resonance frequency which do not exist under white noise excitations due to the constant

mean square value of the excitation in the frequency domain.[1]

The maximum value of the average power occurs when the mean square value of the velocity exhibits a minimum as depicted in Fig. 5(c). This can be further confirmed by minimizing (16b) with respect to α which yields the same expression for α_{opt} as given in (18). One plausible explanation is that maximum electric damping occurs at the point where maximum energy is channeled from the mechanical subsystem. This yields a minimum in the mean square value of the velocity.

It can also be noted that, in general, the output power increases as the stiffness decreases (r increases) for any value of α. When the stiffness decreases, the harvester becomes softer, experiencing larger motions for smaller input excitations. As a result, the mean square value of the displacement increases approaching infinity as the stiffness approaches zero, see also Fig. 5(b). The increased mean square value of the displacement aids in increasing the average output power. However, at the same time, the reduction in stiffness reduces the frequency of oscillation, thereby, reducing the mean square value of the voltage, and, hence, the average power. It turns out that the net increase in the average power due to the increase in the mean square value of the displacement overcomes the decrease due to the reduction in the frequency which causes the average power to increase with r.

5 Energy harvesters with a nonlinear restoring force

For a nonlinear system, an exact solution of the FPK equation, (11), is not always easily attainable even in the stationary sense. The reason being that, even when the input excitation is Gaussian, the response PDF will deviate from the Gaussian distribution depending on the strength of the nonlinearity. For a weakly-nonlinear system, the PDF will be slightly deviated from Gaussian while, for a strongly-nonlinear system, the PDF will be very different from the Gaussian distribution. To approximate the response statistics in such scenarios, it is common to seek an approximate solution of the FPK equation. One approach is based on generating the differential equations governing the response moments (moment differential equations). To that end, we multiply both sides of (11) by $\prod_{i=1}^{3} x_i^{k_i}$ and integrate over the whole domain to obtain

$$\begin{aligned}
&\int_{-\infty}^{\infty}\int_{-\infty}^{\infty}\int_{-\infty}^{\infty}\prod_{i=1}^{3}x_i^{k_i}\frac{\partial P(\mathbf{x},t)}{\partial t}\,\mathrm{d}x_1\mathrm{d}x_2\,\mathrm{d}x_3\\
&\quad=-\int_{-\infty}^{\infty}\int_{-\infty}^{\infty}\int_{-\infty}^{\infty}\prod_{i=1}^{3}x_i^{k_i}\left(x_2\frac{\partial P(\mathbf{x},t)}{\partial x_1}\right)\mathrm{d}x_1\mathrm{d}x_2\,\mathrm{d}x_3\\
&\qquad+2\zeta\int_{-\infty}^{\infty}\int_{-\infty}^{\infty}\int_{-\infty}^{\infty}\prod_{i=1}^{3}x_i^{k_i}\\
&\qquad\times\frac{\partial(x_2P(\mathbf{x},t))}{\partial x_2}\mathrm{d}x_1\mathrm{d}x_2\,\mathrm{d}x_3\\
&\qquad+\int_{-\infty}^{\infty}\int_{-\infty}^{\infty}\int_{-\infty}^{\infty}\prod_{i=1}^{3}x_i^{k_i}\left(\frac{\mathrm{d}U}{\mathrm{d}x_1}+\kappa^2x_3\right)\\
&\qquad\times\frac{\partial P(\mathbf{x},t)}{\partial x_2}\mathrm{d}x_1\mathrm{d}x_2\,\mathrm{d}x_3\\
&\qquad+\alpha\int_{-\infty}^{\infty}\int_{-\infty}^{\infty}\int_{-\infty}^{\infty}\prod_{i=1}^{3}x_i^{k_i}\\
&\qquad\times\frac{\partial(x_3P(\mathbf{x},t))}{\partial x_3}\mathrm{d}x_1\mathrm{d}x_2\,\mathrm{d}x_3\\
&\qquad+\int_{-\infty}^{\infty}\int_{-\infty}^{\infty}\int_{-\infty}^{\infty}\prod_{i=1}^{3}x_i^{k_i}\left(x_2\frac{\partial P(\mathbf{x},t)}{\partial x_3}\right)\mathrm{d}x_1\mathrm{d}x_2\,\mathrm{d}x_3\\
&\qquad+\frac{\sigma^2}{2}\int_{-\infty}^{\infty}\int_{-\infty}^{\infty}\int_{-\infty}^{\infty}\prod_{i=1}^{3}x_i^{k_i}\frac{\partial^2P(\mathbf{x},t)}{\partial^2x_2}\mathrm{d}x_1\mathrm{d}x_2\,\mathrm{d}x_3.
\end{aligned}\tag{19}$$

Integrating each term in (19) by parts while taking into account the boundary conditions, $P(\infty,t)=P(-\infty,t)=0$, yields

$$\begin{aligned}
&\frac{\mathrm{d}m_{k_1,k_2,k_3}}{\mathrm{d}t}\\
&\quad=k_1m_{k_1-1,k_2+1,k_3}+k_3m_{k_1,k_2+1,k_3-1}-\alpha k_3m_{k_1,k_2,k_3}\\
&\qquad-\delta k_2m_{k_1+3,k_2-1,k_3}-2\zeta k_2m_{k_1,k_2,k_3}\\
&\qquad-\kappa^2k_2m_{k_1,k_2-1,k_3+1}-k_2(1-r)m_{k_1+1,k_2-1,k_3}\\
&\qquad+\frac{1}{2}(k_2-1)k_2\sigma^2m_{k_1,k_2-2,k_3},
\end{aligned}\tag{20}$$

where $m_{k_1,k_2,k_3}=\langle\prod_{i=1}^{3}x_i^{k_i}\rangle$ is the statistical moment of order $K=\sum_{i=1}^{3}k_i$. Equations (20) which are also known as the moment differential equations can be simultaneously integrated to study time evolution of the

[1] The reader can refer to Renno et al. [31] for more details on the optimization of energy harvesters under sinusoidal deterministic excitations.

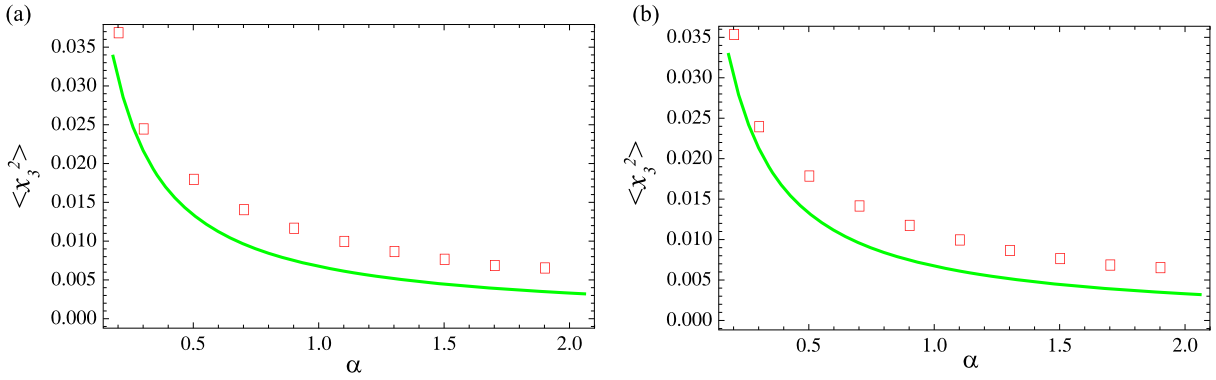

Fig. 6 (**a**) Variation of the mean square voltage with α for a mono-stable system with $r = 0.9$, $\delta = 4$, $\zeta = 0.01$, $\kappa = 0.75$ and $\sigma = 0.09$. (**b**) Variation of the mean square voltage with α for a bi-stable system with $r = 1.1$, $\delta = 4$, $\zeta = 0.01$, $\kappa = 0.75$ and $\sigma = 0.09$. *Squares* represent numerical integration utilizing Matlab Stochastic Communication Toolbox

response statistics for any set of initial conditions. At steady-state, the response statistics are time-invariant which permits setting the left hand-side of (20) equal to zero and solving the resulting algebraic equations together for the steady-state response moments. The stability of the resulting solutions can then be assessed by finding the eigenvalues of the associated Jacobian matrix.

For a linear system subjected to Gaussian excitations, moments of order lower than two, i.e., $K \leq 2$, are independent of higher-order moments. For nonlinear systems, however, similar to the one considered here, the resulting moment equations are coupled to higher-order moments. In (20), the coupling occurs through the term associated with the nonlinearity δ. This yields an infinite hierarchy problem which should be *closed* in an appropriate manner so that the approximate response statistics can be calculated. A proper *closure scheme* truncates the problem into a finite set of equations while preserving the statistical moment properties and Shwarz's inequality ($\langle x \rangle^2 \leq \langle x^2 \rangle < \infty$) as well as leading solutions that are close to those obtained by numerically solving the FPK equation [34].

The cumulant-neglect closure method [34, 35] will be utilized in this paper to close the moment equations by assuming that the response cumulants above a certain threshold are too small when compared to lower-order cumulants[2] and hence can be neglected. This provides additional equations that relate higher-order moments (above the closure level) to lower-order moments (below the closure level). The response cumulants λ_K of order K can be obtained using the following relation:

$$\lambda_K\left[x_1^{k_1} x_2^{k_2} x_3^{k_3}\right] = \frac{1}{\mathrm{i}^K} \frac{\partial^K \ln(F_{\mathbf{x}}(\mathbf{u}))}{\partial u_1^{k_1} \partial u_2^{k_2} \partial u_3^{k_3}}\bigg|_{\mathbf{u}=0}, \tag{21}$$

where $\mathrm{i}^2 = -1$ and $F_{\mathbf{x}}(\mathbf{u})$ is the characteristic function given by

$$\begin{aligned} F_{\mathbf{x}}(\mathbf{u}) &= \left\langle \exp(\mathrm{i}u_1 x_1 + \mathrm{i}u_2 x_2 + \mathrm{i}u_3 x_3) \right\rangle \\ &= 1 + \sum_{j=1}^{\infty} \frac{1}{j!} \left\langle (\mathrm{i}u_1 x_1 + \mathrm{i}u_2 x_2 + \mathrm{i}u_3 x_3)^j \right\rangle. \end{aligned} \tag{22}$$

As shown in Fig. 6, based on comparisons with numerical simulations, a fourth-order cumulant neglect closure scheme, also know as a non-Gaussian closure, yields acceptable results that reflect the general trends while balancing the computational cost. In that scenario, cumulants of order five and six (λ_5 and λ_6) are set equal to zero to relate fifth and sixth order moments (m_{k_1,k_2,k_3}, $K = 5, 6$) to lower-order moments (m_{k_1,k_2,k_3}, $K \leq 4$). This yields a total of 34 differential moment equations, (20), and a total of 49 algebraic equations from the cumulant negligence scheme, (21). A higher-order closure scheme has been shown to yield even more accurate results but is computationally much more expensive.

Since we are interested in the stationary solutions, the differential moment equations are transformed into a set of algebraic equations by setting the time deriva-

[2]Cumulants are used to provide a measure of correlation strength among different random variables [34].

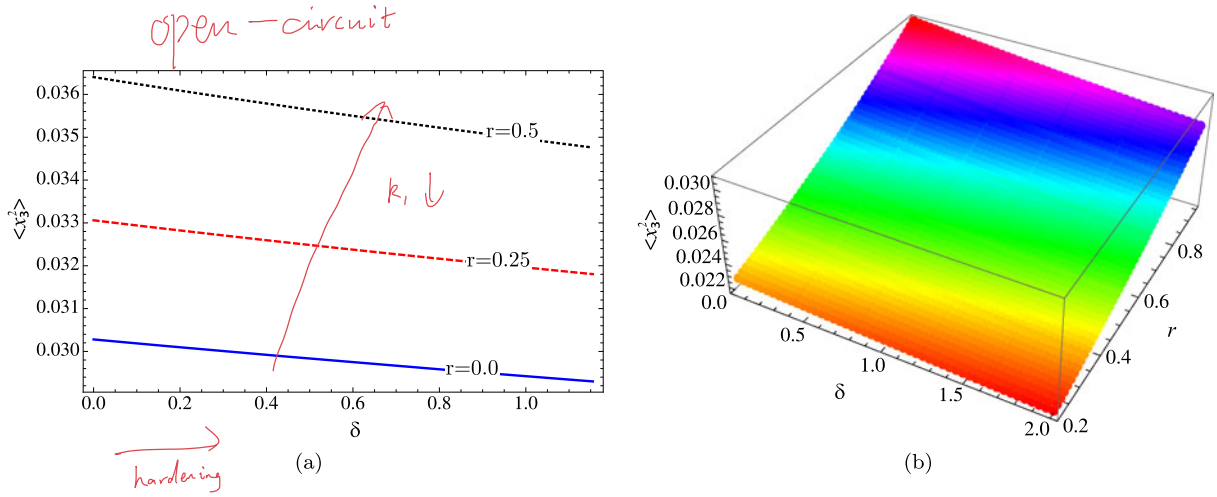

Fig. 7 (**a**) Variation of the mean square voltage with δ for different values of r and $\alpha = 0.05$, $\zeta = 0.01$, $\kappa = 0.75$, and $\sigma = 0.06$. (**b**) Associated surface of the mean square voltage obtained for similar value of the design parameters and $\sigma = 0.05$

tives equal to zero. The resulting 83 coupled algebraic equations are solved together for the response moments. These equations yield a non-unique set of solutions whose stability are assessed using the eigenvalues of the associated Jacobian matrix. Only one of these solutions yields stable, physically realizable, response moments. This represents the only actual and unique solution of the FPK equation. In what follows, we use this unique solution to investigate the influence of nonlinearity on the output power in mono-stable harvesters.

5.1 Nonlinear harvesters with a mono-stable potential function

Figure 7(a) depicts variation of the mean square voltage with the nonlinearity coefficient δ for different values of r and a small value of the time constant ratio, $\alpha = 0.05$ (close to the open-circuit condition). It is evident that, as the nonlinearity increases, the mean square voltage decreases regardless of the value of r. The decrease in the voltage follows a linear trend for the range of the nonlinearity studied. A surface showing variation of the mean square voltage with r and δ is depicted in Fig. 7(b), clearly illustrating that the mean square voltage always decreases with δ for any value of r.

The same conclusion is also deduced when inspecting Fig. 8 which depicts variation of the mean square voltage with δ for a large value of the time constant ratio, $\alpha = 10$ (close to the short-circuit condition). Here,

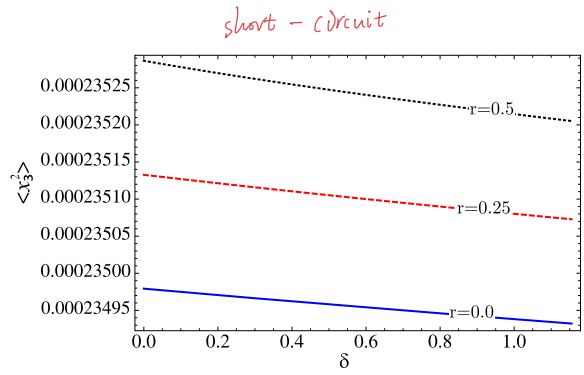

Fig. 8 Variation of the mean square voltage with δ for different values of r and $\alpha = 10$, $\zeta = 0.01$, $\kappa = 0.75$, and $\sigma = 0.06$

however, variation of the voltage with the nonlinearity is very small to the extent that it can be considered negligible.

Figure 9 illustrates variation of the output power with the time constant ratio for the linear harvester, $\delta = 0$, as compared to the nonlinear mono-stable harvester with $\delta = 10, 20$. Again, it is evident that the nonlinearity has an adverse influence on the average output power. The reduction in the average power is mostly pronounced for smaller values of α. The two curves converge to one another as α increases, further emphasizing that the influence of the nonlinearity diminishes with α. This clearly demonstrates that intentional inclusion of stiffness-type nonlinearities in mono-stable VEHs will adversely influence their performance under random excitations that can be approximated as a white Gaussian noise process.

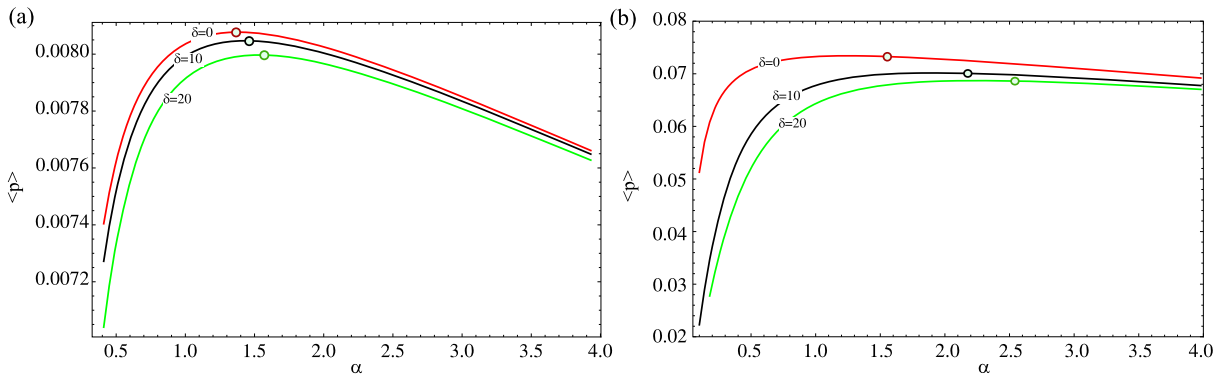

Fig. 9 Variation of the average power with α for different values of δ and $r = 0$, $\zeta = 0.01$, $\kappa = 0.75$. Results are obtained for (**a**) $\sigma = 0.1$ and (**b**) $\sigma = 0.3$. *Circles* represent the optimal value of the time constant ratio, α_{opt}

The larger the nonlinearity is, the smaller the average power will be. Reduction in the output power is mostly pronounced for smaller values of the time constant ratio.

Further inspection of Fig. 9(a) reveals that the optimal time constant ratio which is inversely proportional to the load resistance increases with the nonlinearity. This result can be of importance even for VEHs that do not intentionally incorporate nonlinearities. Specifically, since most VEHs exhibit some inherent stiffness nonlinearities that are usually of the hardening cubic type, the optimal operating electric load should be chosen such that it shifts the time constant ratio of the VEH away from the linear optimal one and towards larger values. This will help increase the average power of typical VEHs when excited by random broadband excitations. Similar trends can be seen in Fig. 9(b) when the variance of the excitation is increased to $\sigma = 0.3$. The main difference is that the optimal time constant shifts even further towards larger values.

5.2 Nonlinear harvesters with a bi-stable potential function

In this section, we treat piezoelectric harvesters with bi-stable potential. The goal is to analyze how the average power of the harvester depends on the potential shape and excitation's intensity as compared to the linear harvester. Here, again, a fourth-order cumulant neglect closure scheme is utilized to obtain the response statistics. We start by investigating how the potential shape influences the mean square voltage of the harvester. Figure 10(a) depicts variation of the mean square voltage with δ for $r = 1.1$ and a small time constant ratio $\alpha = 0.05$. Results indicate that the mean square voltage increases initially with δ then decreases beyond an optimal value, δ_{opt}, which decreases as the noise intensity is increased. To put these results in a better perspective, we show the shape of the potential function for three different values of δ and $r = 1.1$ as depicted in Fig. 10(b). As it can be clearly seen, when δ is increased, the separation distance between the wells which is defined by the location of the system's stable fixed points $x_0 = \pm\sqrt{\frac{r-1}{\delta}}$ decreases. The height of the potential barrier at the unstable saddle, $h_b = \frac{(r-1)^2}{4\delta}$, also decreases, see Fig. 10(c). This creates shallower potential wells, which, in turn, facilitates the transition of dynamic trajectories from one potential well to the other; a phenomenon commonly known as the inter-well dynamics. Activation of the inter-well dynamics, which clearly depends on the excitation intensity, is key towards enhancing the transduction of a bi-stable harvester.

For example, consider the case when $\delta = 4$ as shown in Fig. 10(b). In such a scenario, the inter-well dynamics can be easily activated and the frequency of trajectories' transitions is very high as depicted in the time history shown in Fig. 11(a). However, since the separation distance between the wells is small, the mean square value of the voltage remains small at about $\langle x_3^2 \rangle = 0.1046$. When δ is decreased to $\delta = 1.25$, the inter-well dynamics can still be activated at a high transition frequency, Fig. 11(b). In this case, however, because the separation distance is larger, each transition event produces a larger voltage which helps increase the mean square voltage of the

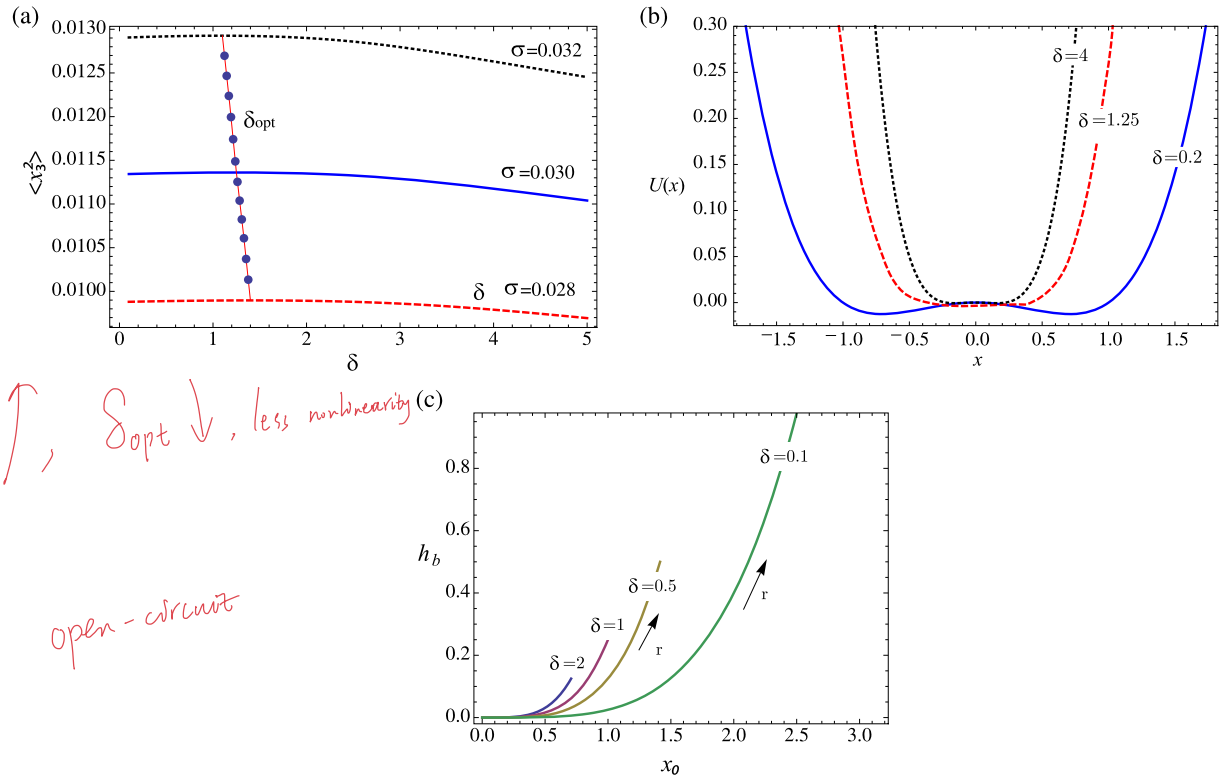

Fig. 10 (**a**) Variation of the mean square voltage with δ for different values of σ and $\alpha = 0.05$, $\zeta = 0.01$, $\kappa = 0.75$, and $r = 1.1$. (**b**) Associated potential energy functions for different values of δ and $r = 1.1$. (**c**) A parametric plot of the potential height versus the separation distance between the wells for different values of δ and $1 < r \leq 2$

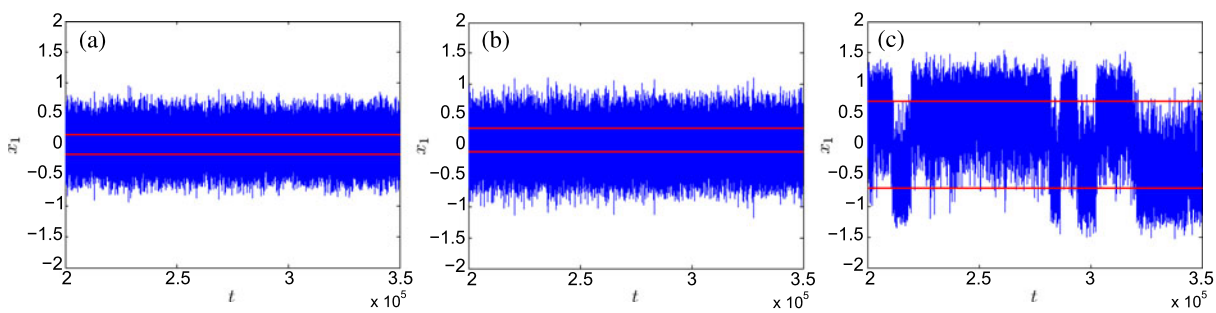

Fig. 11 Displacement time histories for (**a**) $\delta = 4$, (**b**) $\delta = 1.25$, and (**c**) $\delta = 0.2$. Results are obtained for $\sigma = 0.09$, $\alpha = 0.05$, $\zeta = 0.01$, $\kappa = 0.75$, and $r = 1.1$. *Solid lines* represent stable equilibria

response. As such, the effective mean square voltage of the harvester increases to $\langle x_3^2 \rangle = 0.1134$. When the nonlinearity coefficient is decreased further to $\delta = 0.2$, transition of dynamic trajectories becomes very difficult confining the dynamics mostly to one potential well (intra-well response) as shown in Fig. 11(c). This has the adverse influence of reducing the mean square voltage to $\langle x_3^2 \rangle = 0.0979$.

Based on the preceding discussion, it is evident that δ_{opt} represents the value of the nonlinearity which creates a potential function that balances the frequency of transition with the separation distance between the wells to maximize the mean square value of the voltage. This optimal value decreases with the noise intensity, because for a larger intensity, the balance will be maintained for potential functions with higher barriers

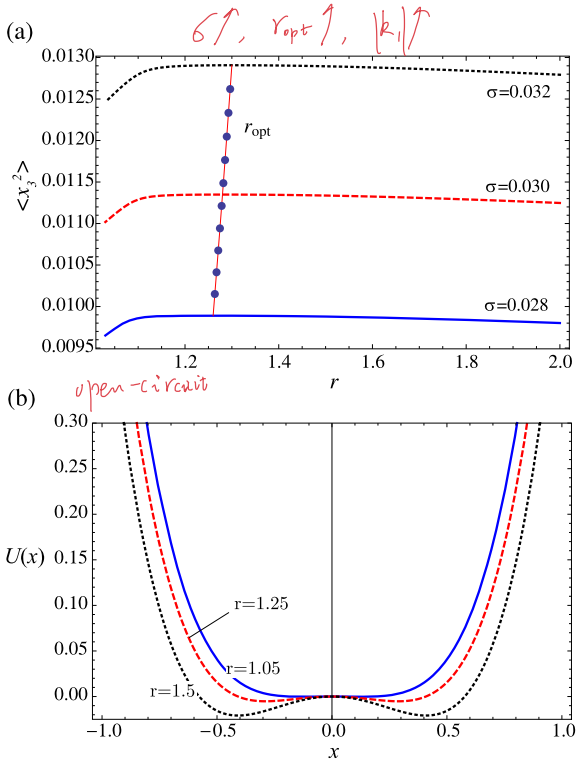

Fig. 12 (**a**) Variation of the mean square voltage with r for different values of σ and $\alpha = 0.05$, $\zeta = 0.01$, $\kappa = 0.75$, and $\delta = 3$. (**b**) Associated potential energy functions for different values of r and $\delta = 3$

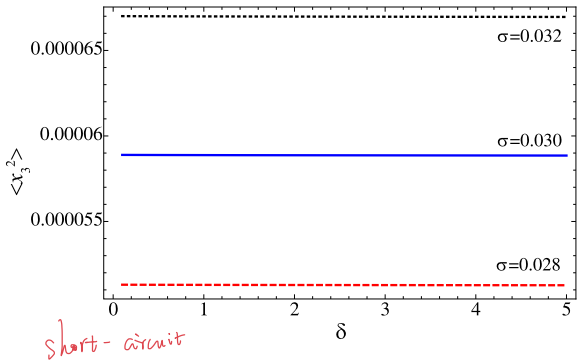

Fig. 13 Variation of the mean square voltage with r for different values of σ and $\alpha = 10$, $\zeta = 0.01$, $\kappa = 0.75$, and $\delta = 3$

and larger separation distances. The same conclusions can also be deduced but in the opposite sense as r is increased for a given δ as can be seen in Figs. 12(a) and 12(b).

Here again it is shown that, when α is large, the potential shape has a very little influence on the output voltage. This is true even for the bi-stable harvester as evident in Fig. 13 which depicts variation of the mean square voltage with δ for $\alpha = 10$.

A clearer picture illustrating the influence of the potential shape on the output voltage can be observed by inspecting the surfaces shown in Figs. 14(a) and 14(b). For a given δ, the mean square voltage increases initially with r but decreases beyond a certain optimal value. This optimal r shifts towards smaller values as δ decreases, approaching one when δ approaches zero. The decrease in the optimal value of r occurs to balance the increase in the height of the potential barrier and the separation between the potential wells due to the increase in δ. Hypothetically, the maximum mean square voltage at this noise intensity occurs when r approaches one and δ approaches zero, i.e., a harvester without a restoring force. This, however, is not physically realizable because it implies that the mean square value of the displacement would approach infinity.

When the noise intensity is reduced by half, similar trends can be seen in Fig. 15(a), with two main differences. First, it can be observed that, for any value of δ, the optimal power is now shifted towards smaller values of r. This is expected due to the decrease in the noise intensity. Second, the power curves are not as sensitive to variations in δ as they are to variation in r leading to the conclusion that, for this small noise intensity, the dynamics does not change significantly as δ is varied within this range.

When the noise intensity is doubled to $\sigma = 0.12$, the power curves become very sensitive to variations in r as observed in Fig. 15(b). In this case, an optimal value of r can be clearly identified. Below that value, there is a sharp decrease in the output power. Although, for small values of r, the inter-well dynamics can be easily activated, the separation distance between the wells becomes too small for this high noise intensity which reduces the output voltage. Beyond the optimal value, the power also decreases but with a much smaller slope. Here, the inter-well dynamics of the harvester is activated less frequently but the separation distance between the wells is large enough to balance this reduction in the frequency.

The preceding results further reiterate an important conclusion concerning the design of a bi-stable energy harvester for random excitation sources. Specifically, the optimal design of the potential shape depends on the excitation intensity. A certain potential shape optimized for a given known noise intensity does not necessarily provide an acceptable performance for other

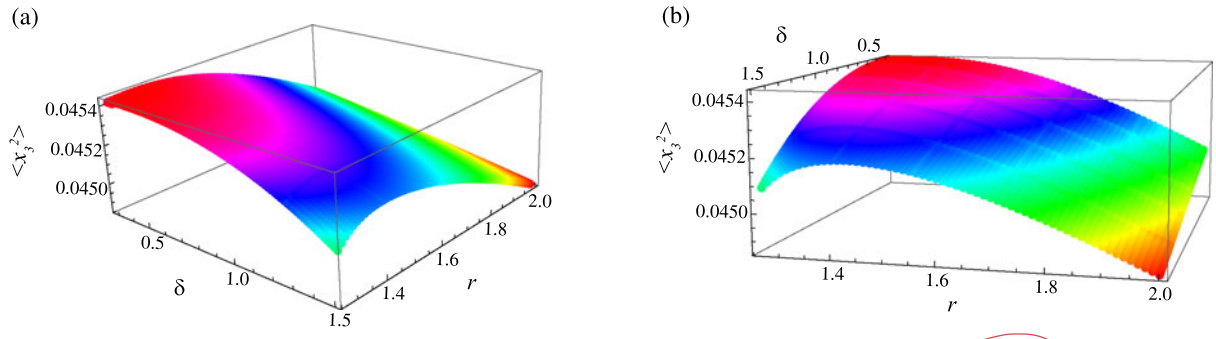

Fig. 14 (**a**), (**b**) Variation of the mean square voltage with r and δ for $\alpha = 0.05$, $\zeta = 0.01$, $\kappa = 0.75$, and $\sigma = 0.06$

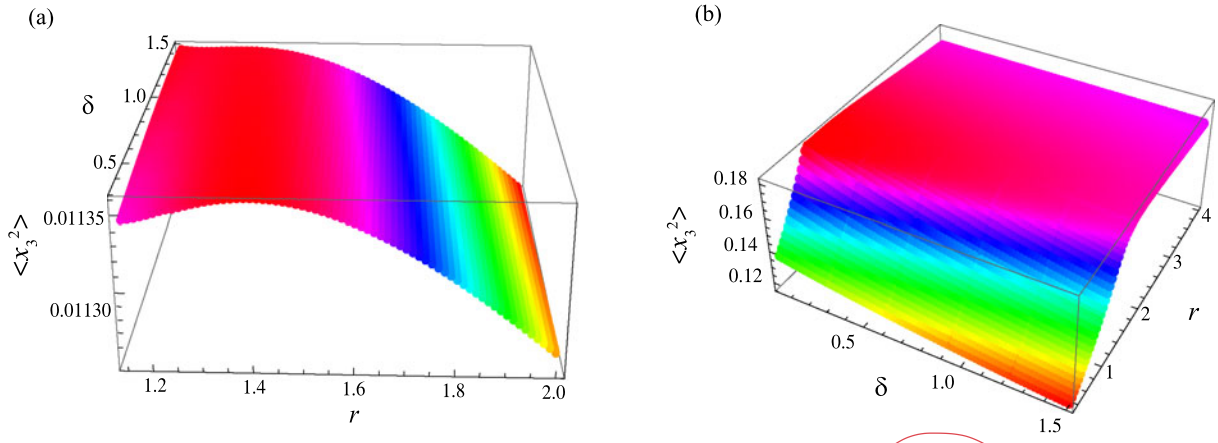

Fig. 15 Variation of the mean square voltage with r and δ for $\alpha = 0.05$, $\zeta = 0.01$, $\kappa = 0.75$, and $\sigma = 0.03$

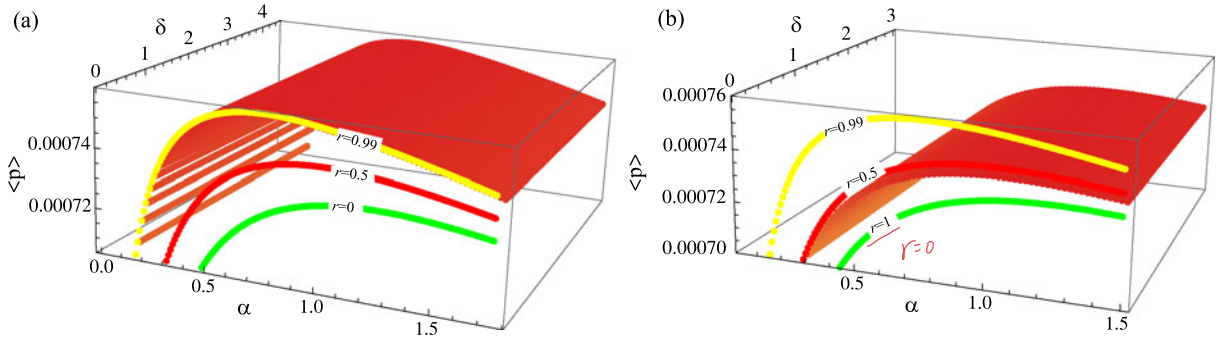

Fig. 16 Variation of the average power with α and δ for $\zeta = 0.01$, $\kappa = 0.75$, and $\sigma = 0.03$. (**a**) $r = 1.4$ and (**b**) $r = 8$

noise intensities further complicating the process of designing bi-stable VEHs with desirable performance characteristics.

Figure 16(a) investigates whether designing a harvester with a bi-stable potential can enhance the transduction under white Gaussian excitations when compared to a linear harvester. The figure depicts variation of the average power with the time constant ratio, α, and the nonlinearity coefficient, δ. An r value of 1.4 was chosen to generate the surface based on the results shown in Fig. 15(a) which demonstrate that this value of r produces maximum power for most values

of δ. As expected, the average power exhibits a maximum value for a given optimal α. Quite interestingly, the nonlinearity coefficient seems to have a very little influence on the average power for this value of r. The surface of average power is compared to average power curves obtained using a linear harvester with three different values of r; namely $r = 0$, 0.5 and 0.99. It is evident that the bi-stable harvester with the optimal design parameters significantly outperforms the linear harvester for $r = 0$ and $r = 0.5$. However, when $r = 0.99$, the linear harvester provides slightly more power than the bi-stable one. It should be borne in mind, however, that designing a harvester very close to a linear instability, i.e., $r \to 1$ and $\delta \to 0$ is very hard to achieve in an experimental setting using tuning mechanisms similar to the ones discussed in the introduction. Furthermore, when r approaches one without the presence of amplitude-limiting nonlinearities, the amplitude of the response unrealistically approaches infinity.

While Fig. 16(a) demonstrates that an energy harvester with a bi-stable potential can outperform a linear harvester, this does not occur for any potential shape. Indeed, for a give noise intensity, only a certain range of r and δ will result in a desirable potential function. To further confirm this conclusion, Fig. 16(b) depicts variation of the average power with the time constant ratio, α, and the nonlinearity coefficient, δ, for $r = 8$, which is far from the optimal value. Here, we can clearly see that the average output power is reduced significantly and a linear harvester with values of r ranging between 0.5 and 1 can clearly outperform the bi-stable design. As such, extreme care should be taken while designing harvesters with bi-stable potential for excitation sources that exhibit the characteristic of white Gaussian noise.

6 Time constant ratio

It is evident through the previous analysis that the time constant ratio, α, plays a critical role in characterizing the influence of the nonlinearity on energy harvesting under white Gaussian excitations. In particular, the affect of the nonlinearity clearly diminishes as the time constant ratio becomes large. From a general point of view, this can be explained by inspecting (4) and noting that the circuit dynamics represents a first-order low-pass filter with the velocity being its input, the voltage representing its output, and α characterizing the inverse of its time constant. When α is large, the bandwidth of the filter is large, and the circuit dynamics can be approximated via $\alpha V = \dot{x}$. This allows the dynamics of the coupled system to be further reduced to the following form:

$$\ddot{x} + \zeta_{\text{eff}}\dot{x} + \frac{\mathrm{d}U}{\mathrm{d}x} = -\ddot{x}_b \tag{23}$$

where $\zeta_{\text{eff}} = 2\zeta + \kappa^2/\alpha$. For the reduced system, the PDF of the response can be obtained by solving the following FPK equation

$$\begin{aligned}\frac{\partial P(\mathbf{x},t)}{\partial t} &= -x_2\frac{\partial P(\mathbf{x},t)}{\partial x_1} + 2\zeta_{\text{eff}}\frac{\partial (x_2 P(\mathbf{x},t))}{\partial x_2} \\ &\quad + \left(\frac{\mathrm{d}U}{\mathrm{d}x_1}\right)\frac{\partial P(\mathbf{x},t)}{\partial x_2} + \frac{\sigma^2}{2}\frac{\partial^2 P(\mathbf{x},t)}{\partial^2 x_2}, \\ P(\infty,t) &= P(-\infty,t) = 0,\end{aligned} \tag{24}$$

where again $(x_1, x_2, x_3)^T \equiv (x, \dot{x}, V)^T$. Equation (24) admits a stationary PDF of the form

$$\begin{aligned}P(x_1,x_2) &= A_1 \exp\left\{\frac{-2\zeta_{\text{eff}}}{\sigma^2}U(x_1)\right\} \\ &\quad \times A_2 \exp\left\{\frac{-2\zeta_{\text{eff}}}{\sigma^2}\frac{x_2^2}{2}\right\},\end{aligned} \tag{25}$$

where $A_1^{-1} = \int_{-\infty}^{\infty}\exp\{\frac{-2\zeta_{\text{eff}}}{\sigma^2}U(x_1)\}\,\mathrm{d}x_1$ and $A_2^{-1} = \int_{-\infty}^{\infty}\exp\{\frac{-2\zeta_{\text{eff}}}{\sigma^2}\frac{x_2^2}{2}\}\,\mathrm{d}x_2$. Note that, in this case, the resulting PDF can be factored into a function of the displacement, x_1, and velocity, x_2. This implies that the displacement and velocity can be treated as two independent random variables. With that, the expected mean square value of the velocity, $\langle x_2^2\rangle$, is independent of the displacement, nonlinearity, and the potential function altogether; and is given by

$$\langle \dot{x}^2\rangle \equiv \langle x_2^2\rangle = A_2\int_{-\infty}^{\infty} x_2^2 \exp\left\{\frac{-\zeta_{\text{eff}}}{\sigma^2}x_2^2\right\}\mathrm{d}x_2 = \frac{\sigma^2}{2\zeta_{\text{eff}}}. \tag{26}$$

For large values of α, i.e., $\kappa^2 \lll \alpha$, the term κ^2/α within ζ_{eff} can also be neglected. In such a case, the expected mean square value of the velocity reduces to $\frac{\sigma^2}{4\zeta}$ which represents the same exact expression one obtains by taking the limit of the mean square velocity, (16a), (16b), (16c), of the linear harvester as α ap-

proaches infinity. This implies that a linear and a nonlinear harvester provide similar mean square velocities for large values of α.

Next, using the relation $V = \dot{x}/\alpha$ in conjunction with (26), the expected value of the mean square voltage and average power can be written as

$$\langle V^2 \rangle \equiv \langle x_3^2 \rangle = \frac{\sigma^2}{2\alpha^2 \zeta_{\text{eff}}}, \qquad \langle \text{p} \rangle = \frac{\sigma^2}{2\alpha \zeta_{\text{eff}}}. \tag{27}$$

The previous expressions are independent of the shape of the potential function. This leads to the conclusion that, under white Gaussian excitations and, for large values of the time constant ratio α, no matter how the potential function of the harvester is altered, it will have no influence on the average output power of the device. This conclusion holds for harvesters with nonlinearities appearing in the restoring force. The author arrived at a similar conclusion in an earlier work on the response of mono-stable inductive harvesters to random broadband excitations, [28]. The basic model adopted in [28] lends itself to a similar form as in (23) because the inductance of the harvesting coil was assumed to be negligible as it is usually the case with inductive-type harvesters.

7 Conclusions

This paper investigated the influence of stiffness-type nonlinearities on the transduction of VEHs under random excitations that can be approximated by a white Gaussian noise process. Both mono- and bi-stable piezoelectric Duffing-type harvesters are considered. The FPK equation governing the evolution of the system's transition probability density function is formulated and used to generate the moment differential equations governing the response statistics. For the nonlinear VEHs, the moment equations are then closed using a fourth-order cumulant-neglect closure scheme and the relevant steady-state response statistics are obtained. The influence of the nonlinearity, time constant ratio, and noise intensity on the mean square voltage and average power is detailed. Results are then compared with those obtained by analytically solving the FPK equation for the linear resonant harvester leading to the following conclusions:

- A nonlinear mono-stable Duffing-type harvester can never outperform its linear counterpart regardless of the linear stiffness or noise intensity. The larger the coefficient of the cubic nonlinearity is, the lower is the average output power.
- The time constant ratio, i.e., ratio between the period of the mechanical subsystem and the time constant of the harvesting circuit, plays a critical role in characterizing the influence of stiffness nonlinearities on the average power.
- When the time constant ratio is large, the influence of the nonlinearity diminishes, and both a linear and a nonlinear harvester provide the same value of average power regardless of the noise intensity. In such a case, no matter how the potential function of the harvester is altered, it has no influence on the average output power of the device. This conclusion holds for any harvester with nonlinearities appearing in the restoring force.
- When the time constant ratio is small, a mono-stable Duffing-type harvester always produces less power than the linear one. A bi-stable duffing harvester can, for some optimal potential shapes, outperform the linear harvester. The potential function's optimal shape balances the transitional frequency of the dynamic trajectories between its wells and their separation distance to maximize the mean square value of the voltage.
- For bi-stable harvesters, the shape of the optimal potential function is sensitive to the noise intensity further complicating the design of efficient bi-stable VEHs for random excitations with unknown and variable noise intensity.
- To enhance the transduction of energy harvesters under white Gaussian excitations, other types of nonlinearities, e.g., nonlinearities in the harvesting circuit dynamics or in the velocity should be investigated.

Acknowledgements This material is based upon work supported by the National Science Foundation under CAREER Grant No. 1055419. Any opinions, findings, and conclusions or recommendations expressed in this material are those of the author and do not necessarily reflect the views of the National Science Foundation.

References

1. Roundy, S., Wright, P.K., Rabaey, J.: A study of low level vibrations as a power source for wireless sensor nodes. Comput. Commun. **26**, 1131–1144 (2003)

2. Roundy, S., Zhang, Y.: Toward self-tuning adaptive vibration-based micro-generators. In: Smart Materials, Nano- and Micro-Smart Systems, Sydney, Australia (2005)
3. Wu, W., Chen, Y., Lee, B., He, J., Peng, Y.: Tunable resonant frequency power harvesting devices. In: Proceedings of Smart Structures and Materials Conference, SPIE, San Diego, CA, p. 61690A (2006)
4. Challa, V., Prasad, M., Shi, Y., Fisher, F.: A vibration energy harvesting device with bidirectional resonance frequency tunability. Smart Mater. Struct. **75**, 1–10 (2008)
5. Shahruz, S.M.: Design of mechanical band-pass filters for energy scavenging. J. Sound Vib. **292**, 987–998 (2006)
6. Shahruz, S.M.: Limits of performance of mechanical band-pass filters used in energy harvesting. J. Sound Vib. **294**, 449–461 (2006)
7. Baker, J., Roundy, S., Wright, P.: Alternative geometries for increasing power density in vibration energy scavenging for wireless sensors. In: Proceedings of the Third International Energy Conversion Conference, San Francisco, CA, pp. 959–970 (2005)
8. Rastegar, J., Pereira, C., Nguyen, H.L.: Piezoelectric-based power sources for harvesting energy from platforms with low frequency vibrations. In: Proceedings of Smart Structures and Materials Conference, SPIE, San Diego, CA, p. 617101 (2006)
9. McInnes, C.R., Gorman, D.G., Cartmell, M.P.: Enhanced vibrational energy harvesting using nonlinear stochastic resonance. J. Sound Vib. **318**, 655–662 (2008)
10. Barton, D., Burrow, S., Clare, L.: Energy harvesting from vibrations with a nonlinear oscillator. J. Vib. Acoust. **132**, 0210091 (2010)
11. Mann, B., Sims, N.: Energy harvesting from the nonlinear oscillations of magnetic levitation. J. Sound Vib. **319**, 515–530 (2008)
12. Masana, R., Daqaq, M.F.: Electromechanical modeling and nonlinear analysis of axially-loaded energy harvesters. J. Vib. Acoust. **133**, 011007 (2011)
13. Quinn, D., Triplett, L., Vakakis, D., Bergman, L.: Comparing linear and essentially nonlinear vibration-based energy harvesting. J. Vib. Acoust. **133**, 011001 (2011)
14. Erturk, A., Hoffman, J., Inman, D.J.: A piezo-magnetoelastic structure for broadband vibration energy harvesting. Appl. Phys. Lett. **94**, 254102 (2009)
15. Cottone, F., Vocca, H., Gammaitoni, L.: Nonlinear energy harvesting. Phys. Rev. Lett. **102**, 080601 (2009)
16. Daqaq, M.F., Stabler, C., Seuaciuc-Osorio, T., Qaroush, Y.: Investigation of power harvesting via parametric excitations. J. Intell. Mater. Syst. Struct. **20**, 545–557 (2009)
17. Stanton, S.C., McGehee, C.C., Mann, B.P.: Nonlinear dynamics for broadband energy harvesting: investigation of a bistable piezoelectric inertial generator. Physica D, Nonlinear Phenom. **239**, 640–653 (2010)
18. Daqaq, M.F., Bode, D.: Exploring the parametric amplification phenomenon for energy harvesting. J. Syst. Control Eng. **225**, 456–466 (2010)
19. Abdelkefi, A., Nayfeh, A.H., Hajj, M.: Global nonlinear distributed-parameter model of parametrically excited piezoelectric energy harvesters. Nonlinear Dyn. **67**(2), 1147–1160 (2011)
20. Abdelkefi, A., Nayfeh, A.H., Hajj, M.: Effects of nonlinear piezoelectric coupling on energy harvesters under direct excitation. Nonlinear Dyn. **67**(2), 1221–1232 (2011)
21. Mann, B.P., Owens, B.A.: Investigations of a nonlinear energy harvester with a bistable potential well. J. Sound Vib. **329**, 1215–1226 (2010)
22. Moon, F.C., Holmes, P.J.: A magnetoelastic strange attractor. J. Sound Vib. **65**, 275 (2009)
23. Masana, R., Daqaq, M.F.: Relative performance of a vibratory energy harvester in mono- and bi-stable potentials. J. Sound Vib. (2011). doi:10.1016/j.jsv.2011.07.031
24. Masana, R., Daqaq, M.F.: Exploiting super-harmonic resonances of a bi-stable axially-loaded beam for energy harvesting under low-frequency excitations. In: Proceedings of the ASME 2011 International Design Engineering Technical Conference and Computers and Information in Engineering Conference, Washington, DC (2011)
25. Adhikari, S., Friswell, M.I., Inman, D.J.: Piezoelectric energy harvesting from broadband random vibrations. Smart Mater. Struct. **18**, 115005 (2009)
26. Seuaciuc-Osorio, T., Daqaq, M.F.: Energy harvesting under excitations of time-varying frequency. J. Sound Vib. **329**, 2497–2515 (2010)
27. Barton, D., Burrow, S., Clare, L.: Energy harvesting from vibrations with a nonlinear oscillator. In: Proceedings of the ASME 2009 International Design Engineering Technical Conference and Computers and Information in Engineering Conference, San Diego, CA (2009)
28. Daqaq, M.F.: Response of uni-modal duffing type harvesters to random forced excitations. J. Sound Vib. **329**, 3621–3631 (2010)
29. Gammaitoni, L., Neri, I., Vocca, H.: Nonlinear oscillators for vibration energy harvesting. Appl. Phys. Lett. **94**, 164102 (2009)
30. Daqaq, M.F.: Transduction of a bistable inductive generator driven by white and exponentially correlated Gaussian noise. J. Sound Vib. **330**, 2554–2564 (2011)
31. Renno, J., Daqaq, M.F., Inman, D.J.: On the optimal energy harvesting from a vibration source. J. Sound Vib. **320**, 386–405 (2009)
32. Ito, K.: Stochastic integral. Proc. Imp. Acad. (Tokyo) **20**, 519–524 (1944)
33. Jazwinski, A.H.: Stochastic Processes and Filtering Theory. Academic Press, San Diego (1970)
34. Ibrahim, R.A.: Parametric Random Vibrations. Research Studies Press, New York (1985)
35. Wojtkiewicz, S., Spencer, B., Bergman, L.A.: On the cumulant-neglect closure method in stochastic dynamics. Int. J. Non-Linear Mech. **95**, 657–684 (1995)